



Enhanced thermal stability of nanocrystalline Cu composites processed by high-pressure torsion: The pinning effect of Al₂O₃, GO, and rGO/Al₂O₃ nanoparticles

Piotr Bazarnik^a, Maria Emerla^{a,*}, Yi Huang^b, Anita Wojciechowska^a, Marta Ciemiorek^a, Wiktor Bednarczyk^c, Agnieszka Jastrzębska^d, Małgorzata Lewandowska^a, Terence G. Langdon^e

^a Warsaw University of Technology, Faculty of Materials Science and Engineering, Woloska 141, Warsaw 02-507, Poland

^b Department of Design and Engineering, Faculty of Science and Technology, Bournemouth University, Poole, Dorset BH12 5BB, United Kingdom

^c Faculty of Metals Engineering and Industrial Computer Science, AGH University of Krakow, al. A. Mickiewicza 30, Krakow 30-059, Poland

^d Warsaw University of Technology, Faculty of Mechatronics, św. Andrzeja Boboli 8, Warsaw 02-525, Poland

^e Department of Aerospace & Mechanical Engineering University of Southern California, Los Angeles, CA 90089-1453, USA

ARTICLE INFO

Keywords:

Aluminium oxide
Graphene oxide
High-pressure torsion
Metal matrix composites
Reduced graphene oxide
Thermal stability

ABSTRACT

Metal matrix composites with improved mechanical properties and thermal stability were produced using mechanical milling, spark plasma sintering (SPS) and high-pressure torsion (HPT). Three types of reinforcing particles were used, i.e., GO, Al₂O₃ and rGO/Al₂O₃. All of the produced composites exhibit higher hardness and tensile strength than pure copper, reaching values of 250 Hv for Cu-GO, 240 Hv for Cu-Al₂O₃, 210 Hv for Cu-rGO/Al₂O₃ and 185 Hv for Cu after HPT. STEM analyses reveal that the HPT significantly refines the grain size of pure copper to ~210 nm, and even more in the Cu-based composites achieving grain sizes as small as ~55–75 nm. Pure Cu after HPT recrystallizes after annealing at 573 K. The Cu-Al₂O₃ composite demonstrated the best thermal stability with a hardness after annealing at 773 K of 220 Hv and a grain size of ~100 nm. The composite of Cu-GO after annealing at 773 K showed slight grain growth up to ~150 nm. The composite Cu-GO/Al₂O₃ exhibits improved microhardness and tensile strength up to 673 K and annealing of this composite at 773 K which led to a bimodal microstructure. All of the composites annealed at 773 K showed hardness above 180 Hv.

1. Introduction

Pure copper exhibits excellent electrical and thermal conductivity which makes it an optimum material for electrical applications. Unfortunately, its tensile properties and hardness are relatively low, and this restricts its use in more advanced applications. One of the possible ways to improve the strength of pure copper, and at the same time to maintain a reasonably high electrical conductivity, lies in refining the grain size [1,2]. Materials with ultrafine (below 1 μm) or nanocrystalline (below 100 nm) grains are most often produced by severe plastic deformation (SPD) techniques such as equal channel angular pressing (ECAP) [3], accumulative roll bonding (ARB) [4] and high-pressure torsion (HPT) [5,6] with the latter considered as the most efficient in terms of the final grain size [7–9]. Earlier studies of copper deformed by various SPD methods showed that the grain size reduction in these methods

produced a significant increase in hardness (by about 270 %) with only a slight decrease in electrical conductivity (by about 12 %) [10].

Despite great improvement in the microhardness and tensile strength, the ultrafine grained (UFG) and nanocrystalline (NC) metals are inherently thermally unstable due to the high energy stored in the form of dislocations and grain boundaries. Thus, in practice UFG and NC metals exhibit a strong tendency for recrystallization at relatively low temperatures compared to their coarse-grained equivalents [11–15] thereby limiting their potential industrial applications at elevated temperatures. Several concepts were proposed to improve the thermal stability of UFG materials but the most promising is to create metal matrix composites (MMCs) by adding thermally stable nanosized particles and uniformly distributing them within the metal matrix [16–19]. These thermally stable nanoparticles have a strong pinning effect which blocks the movement of grain boundaries during annealing and thus limits the

* Corresponding author.

E-mail address: maria.wolna.dokt@pw.edu.pl (M. Emerla).

<https://doi.org/10.1016/j.jalcom.2025.181283>

Received 27 March 2025; Received in revised form 7 May 2025; Accepted 28 May 2025

Available online 29 May 2025

0925-8388/© 2025 The Author(s). Published by Elsevier B.V. This is an open access article under the CC BY-NC license (<http://creativecommons.org/licenses/by-nc/4.0/>).

recrystallization and grain growth processes [20–24].

There are a number of investigations on the fabrication of UFG/NC MMCs but they were mostly reinforced with different types of oxides such as Al_2O_3 [16,25–27] or carbides such as SiC [28–30]. Recently, carbon-based nano-particles have attracted growing attention due to their potential to strongly improve the mechanical properties, promote grain refinement, stabilise the microstructure during annealing and at the same time increase the electrical and thermal properties [31]. As a result, MMCs reinforced with carbon nanotubes (CNTs) [32–34], graphene [35–37] and graphene oxide (GO) [38,39] have been successfully synthesized. However, there are drawbacks regarding the fabrication of carbon reinforced MMCs. In particular, CNTs and graphene flakes exhibit low wettability by metals, which leads to a strong tendency to form agglomeration in the metal matrix [31,40]. Nevertheless, due to the presence of oxygen functional groups GO particles are a promising material to fabricate composites with a good distribution and connection of particles with the matrix [31]. It was shown that oxygen groups on the surface of GO also enhance the connection between GO and metal through the formation of oxygen-mediated chemical bonds which are stronger than conventional adhesive bonding between the graphene and the metal [41–43]. However, it should be emphasized that GO exhibits a lower thermal resistance than graphene and decomposes in the air atmosphere in the temperature range of 573 K – 673 K [44–46]. No results are at present available to establish the behaviour of GO in the composite when heated to such temperatures.

GO flakes can be stabilized by covalent bonding with other nanoparticles such as Au [47], Ag [48], Cu [38], TiO_2 [49] or Al_2O_3 [50] and forming a core-shell structure. The stabilization with Al_2O_3 seems to be very promising since GO has a number of functional groups capable of forming the aluminium–oxygen bonds, such as $\text{C}=\text{O}$ (1730 cm^{-1}), $\text{C}-\text{O}-\text{C}$ (1280 cm^{-1}) and $\text{C}-\text{O}$ (1225 cm^{-1}) as measured on FTIR and Raman [50]. It was shown that the intensities of these peaks decreased due to the formation of the $\text{Al}-\text{O}$ bond that stabilized the GO structure [50]. In addition, this functionalization leads to reduction of GO and formation of reduced GO (rGO). The rGO/ Al_2O_3 composite nanoparticles are a new type of material that have not been tested yet as a filler to form composites, especially the composites having a UFG/NC structure.

Therefore, the purpose of the present study was to fabricate novel thermally stable Cu-based nanocomposites using HPT processing and to investigate the effect of three different types of reinforcement, i.e., Al_2O_3 , GO and modified rGO/ Al_2O_3 , on the microstructural development, the mechanical properties and the thermal stability.

2. Experimental

The following three types of composites were produced in this study containing 1 wt% of nanofillers: Cu-GO, Cu- Al_2O_3 and Cu-rGO/ Al_2O_3 . The GO and Al_2O_3 represent 2D and 3D nanofillers, respectively, whereas the rGO/ Al_2O_3 is a mixture of both. A regular-shaped copper powder (produced by ABCR company) with a purity of 99 % was used as the matrix. All nano-fillers were synthesized at Warsaw University of Technology using the methods described in earlier reports for GO [51], rGO/ Al_2O_3 [50] and Al_2O_3 [52]. The average nanoparticle size measured from SEM images was $150 \pm 16\text{ nm}$, $230 \pm 50\text{ nm}$ and $50 \pm 20\text{ nm}$ for the GO, rGO/ Al_2O_3 and Al_2O_3 , respectively.

The composites were manufactured using the procedure of the mechanical milling of powders followed by sintering using Spark Plasma Sintering (SPS) and subsequent processing by HPT. The mechanical milling of copper powders with selected particles was performed in a planetary ball milling system (Retsch PM100) in a protective argon atmosphere. The processing parameters for the ball milling were a speed of rotation of 300 rpm, a grinding time of 1 h and a weight ratio of powder to balls of 1:10. The material for the milling chamber and balls was ZrO_2 . Mixed powders were sintered using the SPS method with a 10 mm diameter graphite mould. The process was carried out in a

protective argon atmosphere with a heating rate of 373 K/min and the maximum sintering temperature was 1223 K at which the samples were held for 15 min under a pressure of 50 MPa. The material obtained after sintering was cut into discs of 10 mm in diameter and 1 mm in height and the surfaces of these discs were levelled by grinding on 800 papers. The discs were subjected to HPT processing under a compressive pressure of 6 GPa at room temperature with a rotation speed of 1 rpm. Each sample was processed to 20 revolutions through HPT processing using quasi-constrained conditions where there is a small outflow of material around the periphery of the disk during the HPT operation [53]. Additionally, a reference sample of pure copper was produced under the same conditions as the composites.

The fabricated composites were studied in terms of the microstructure using scanning electron microscopy (SEM) (Hitachi SU8000). Observations were conducted in the secondary electron (SE) and backscattered electron (BSE) modes. All observations were carried out on the cross-sectional surfaces of the disc from an area approximately 1 mm from the edge of each disc. The surface of the samples for the SEM observations was prepared by ion milling using a Hitachi IM4000 instrument. Ion polishing is a method that produces a very high-quality surface that is free of surface deformation, stresses or oxide layers and which allows a study of the grain structure and the distribution of particle agglomerates using channel contrast in the SEM.

More detailed observations of the microstructure were carried out using a Thermo-Fisher Scientific SPECTRA 200 scanning transmission electron microscope (STEM) operating at an accelerating voltage of 200 kV and equipped with Super-X energy dispersion spectroscopy (EDX) detectors which permitted additional chemical analyses of the samples. The thin samples for STEM observations were cut using a focused ion beam (FIB) microscope Hitachi NB-5000.

The average grain size of the composites and copper was determined from STEM and SEM images. Visible grain boundaries were marked in ImageJ software, which then calculated the area of each grain and its equivalent diameter. Based on the measurement of at least 150 grains, the average value of the equivalent diameter of the grains of the material was determined. The term grain size, used in this article, means the value of the average equivalent diameter of the grains of a particular material.

The mechanical properties of the composites after HPT processing were studied by microhardness measurements and tensile tests. The Vickers microhardness was measured using a Falcon 503 microhardness tester with a load of 200 g and dwelling time of 10 s. The hardness was measured on the polished disc surfaces along radial directions with a spacing of 0.3 mm between indentations. The tensile tests were performed on miniature tensile specimens cut from the discs via electrical discharge. A Zwick Z005 universal testing machine with an initial strain rate of 10^{-3} s^{-1} was used and at least two tensile specimens were prepared and tested for each material. The gauge length of the tensile specimen was 4 mm, and the cross-sectional dimensions were $0.6 \times 0.8\text{ mm}^2$. A Digital Image Correlation system was employed during the tests to precisely measure the elongations.

The thermal stability of the produced composites was evaluated by annealing the samples in the temperature range from 373 K to 773 K for 1 hour. The annealing time and temperature range were established on the basis of previous studies [54]. After annealing, the samples were evaluated in terms of the microhardness and microstructural changes in the same way as for the composites after HPT. For the sample annealed at 773 K, Electron Backscatter Diffraction (EBSD) measurements were made using Hitachi SU-70 analytical microscope. The accelerating voltage was 25 kV, the working distance was 20 mm, the step size was 40 nm and the map size was $51 \times 38\text{ }\mu\text{m}^2$.

3. Results

3.1. Microstructure

Fig. 1 shows representative SEM BSE micrographs of the fabricated nanocomposites and Cu reference sample after HPT. In practice, the HPT processing led to significant grain size refinement in all materials. The average grain size in pure copper was ~ 210 nm (Fig. 1a) while for the nanocomposites the grain size was much smaller and cannot be determined from these images. However, there are clear agglomerates of nanoparticles whose size and volume fraction depend on the type of filler. For the Cu-GO composite (Fig. 1b) the visible agglomerates cover about 1 % of the sample area and their average size is 200 ± 160 nm. In the case of the Cu-Al₂O₃ composite (Fig. 1c), the volume fraction of agglomerates is smaller at about 0.5 % and their average size is 120 ± 45 nm. For the Cu-rGO/Al₂O₃ composite (Fig. 1d), the agglomerates cover more than 2.5 % of the entire image surface and their average size is about 290 ± 160 nm. Moreover, in the Cu-GO and Cu-Al₂O₃ composites the agglomerates are uniformly distributed over the entire composites (Fig. 1b and c) whereas in the Cu-rGO/Al₂O₃ composite they tend to be grouped into bands (Fig. 1d).

STEM analysis was conducted to analyse the grain structure in detail and nanoparticle distributions in the composites after 20 HPT turns. Obtained results are presented in Figs. 2–4. In all cases the STEM images in bright field (BF) mode show significant grain refinement in the matrix structure. The average grain sizes of the composites were estimated to be ~ 55 , ~ 65 and ~ 75 nm for Cu-GO (Fig. 2a), Cu-Al₂O₃ (Fig. 3a), and Cu-rGO/Al₂O₃ (Fig. 4a), respectively. By contrast, the HPT-processed pure Cu has an average grain size of ~ 210 nm, as shown in Fig. 1a. Obviously, the addition of the GO, Al₂O₃ and rGO/Al₂O₃ nanofillers led to a greater grain size reduction in the Cu matrix than in pure Cu processed by HPT. The images of Figs. 2b, 3b and 4b also show the distribution of nanoparticles in the matrix. Apart from the large agglomerates visible in the SEM BSE images (Fig. 1b-d), a large fraction of the nanoparticles is homogeneously distributed in copper in the form of either individual nanoparticles or small agglomerates having average sizes of ~ 6.5 , ~ 7.0 and ~ 12.0 nm for the Cu-Al₂O₃, Cu-GO and Cu-rGO/Al₂O₃ composites,

respectively.

It is worth noting that, despite the application of intensive plastic deformation via mechanical milling and HPT processing during the synthesis of these nanocomposites, the fillers largely remain intact and do not undergo significant degradation. The EDX chemical distribution maps (Figs. 2c, 3c, 4c) confirm that the chemical compositions of the observed nanoparticles and the agglomerates correspond to the composition of the added fillers. For the Cu-GO (Fig. 2c) and Cu-Al₂O₃ (Fig. 3c) composites, the EDX maps show that the C, O and Al elements are precisely located where the nanoparticles were observed in the HAADF images. In the rGO/Al₂O₃ composite (Fig. 4), the chemical composition of the nanoparticles varies. Some particles contain C, Al and O elements especially in agglomerates whereas others contain only C or only Al and O. This suggests that, in this composite, the Al₂O₃ nanoparticles may have been torn off from the rGO/Al₂O₃ flakes during the HPT processing. At the same time, the intensive deformation does not destroy the GO structure, as confirmed in an earlier study using Raman spectroscopy [54].

3.2. Mechanical properties

The microhardness measurement results are presented in Fig. 5 as a function of the distance from the disc centres. Starting from the results for pure Cu, the microhardness of the samples processed by HPT is more than 100 Hv units higher than the microhardness of the copper in the coarse-grained state after SPS. All of the produced composites exhibit higher microhardness than for Cu after HPT. The highest microhardness values were achieved for the composite with the addition of GO nanoflakes where it is more than 250 Hv units. The lowest hardness value among the composites was obtained for Cu-rGO/Al₂O₃, while the average hardness obtained for this sample was 210 Hv. Moreover, the Cu-GO composite exhibits a homogeneous distribution of microhardness results across the entire disc diameter which indicates that the grain refinement level and the distribution of the nanofillers are quite homogeneous throughout the sample. Composites with the addition of Al₂O₃ and rGO/Al₂O₃ exhibit a small but gradual increase in the microhardness values from the central region to the edge from 220 Hv to

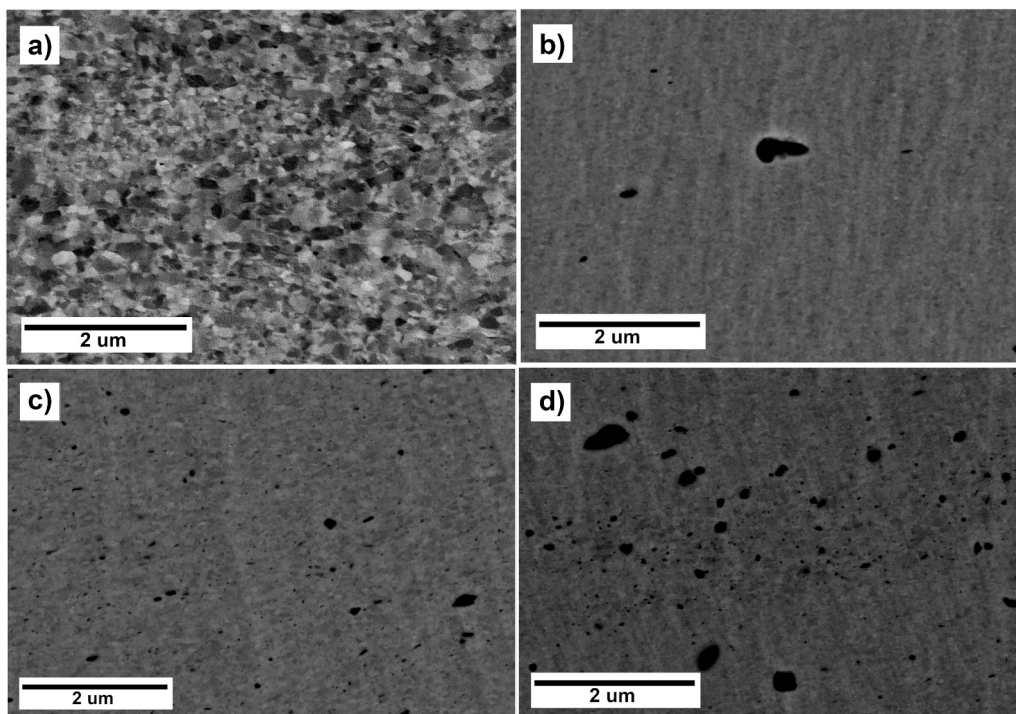


Fig. 1. SEM BSE image of a) Cu after HPT; b) Cu-GO after HPT; c) Cu-Al₂O₃ after HPT; d) Cu-rGO/Al₂O₃ after HPT.

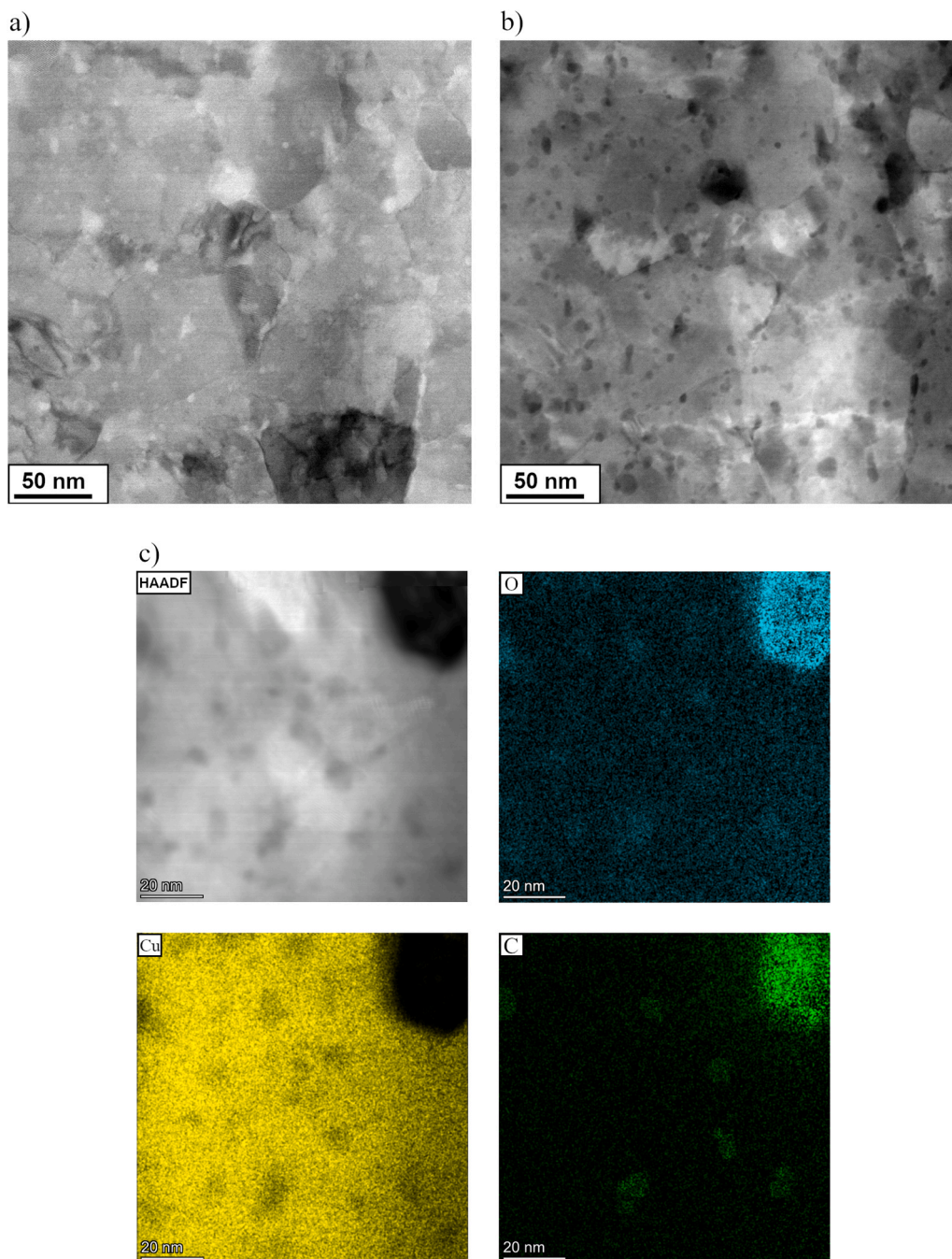


Fig. 2. STEM image of Cu-GO a) bright field, b) HAADF image, c) EDX map.

245 Hv and 190 Hv to 225 Hv, respectively.

The results of the tensile testing for the HPT-processed composite materials are illustrated in Fig. 6. The ultimate tensile strength (UTS) of the HPT-processed pure Cu is ~ 640 MPa which in general is consistent with the available published data [55]. The UTS of the coarse-grained copper after SPS is ~ 250 MPa. The results for the composite samples clearly demonstrate the beneficial role of the nanofillers since the strength consistently increases compared with pure Cu. A highest UTS of $\sim 780 \pm 12$ MPa was recorded for the Cu-Al₂O₃ composite which was a value higher by ~ 140 MPa than for HPT-processed Cu and $\sim 500 \pm 2$ MPa higher than for coarse-grained Cu. The Cu-rGO/Al₂O₃ and Cu-GO composites exhibit slightly lower values of UTS of $\sim 690 \pm 5$ MPa and $\sim 675 \pm 2$ MPa, respectively. Nevertheless, the high strength of the composites is at the expense of ductility since the elongation to failure is

smaller than 10 % and the Cu-GO composite exhibits brittle fracture in the elastic region.

3.3. Thermal stability

Fig. 7 presents the changes in hardness measured at the disc edges for the nanocomposites after 20 HPT turns with subsequent annealing at temperatures ranging from 373 K to 773 K for 1 h. These results are also complemented with the microhardness changes for the Cu HPT sample. The results show that the Cu HPT sample is thermally stable up to 473 K which agrees with published data [40]. The microhardness decreases dramatically from ~ 170 Hv units to ~ 110 Hv units after annealing at 573 K.

By contrast, the microhardness of the fabricated nanocomposites

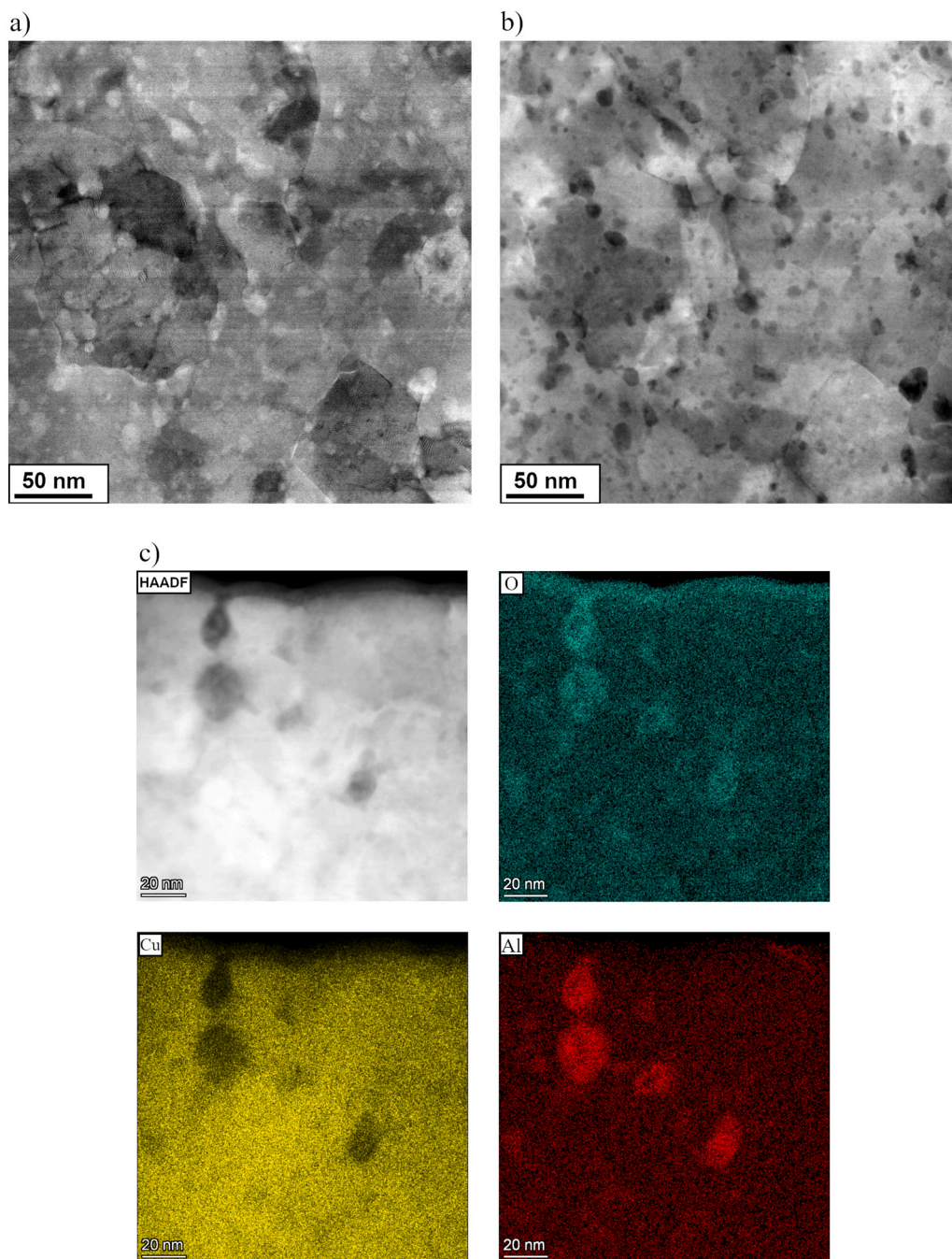


Fig. 3. STEM image of Cu-Al₂O₃ a) bright field, b) HAADF image, c) EDX map.

does not decrease significantly even after annealing at 773 K. Furthermore, even if a drop of microhardness is observed at a higher temperature, the microhardness values are higher than the microhardness of the HPT-processed pure Cu without any post-HPT annealing. In the Cu-GO composite, a gradual decrease in microhardness is observed with increasing annealing temperature but this drop is no larger than ~60 Hv for 773 K. On the other hand, the Cu-Al₂O₃ nanocomposite demonstrates excellent thermal stability with the hardness values remaining steady at ~240 Hv across the entire temperature range. An interesting result was observed in the Cu-rGO/Al₂O₃ composite, for which the microhardness values are stable up to 573 K and after annealing at 773 K the microhardness drops to ~185 Hv units which remains higher than for the Cu HPT sample.

To understand the thermal stability of the HPT-processed

nanocomposites, SEM and STEM studies of the annealed samples were carried out. Fig. 8 shows representative SEM images taken in tunnelling contrast to study grain size coarsening during annealing. The reference Cu HPT sample undergoes recrystallization during annealing at 573 K, leading to the formation of grains which are larger than 100 μm (Fig. 8a). By contrast, the microstructures of the Cu-GO and Cu-Al₂O₃ nanocomposites remain relatively stable at high temperatures (Figs. 8b and 8c). However, in the Cu-GO sample a slight grain coarsening is observed after annealing at 773 K (Fig. 8b) whereas this is not evident for the Cu-Al₂O₃ composite. The Cu-rGO/Al₂O₃ composite after annealing at 773 K exhibits abnormal grain growth leading to the formation of a distinct heterostructure (Fig. 8d). The microstructure in this sample consists of large grains having sizes above ~100 μm and these are surrounded by regions of nanocrystalline grains. Additionally, these large

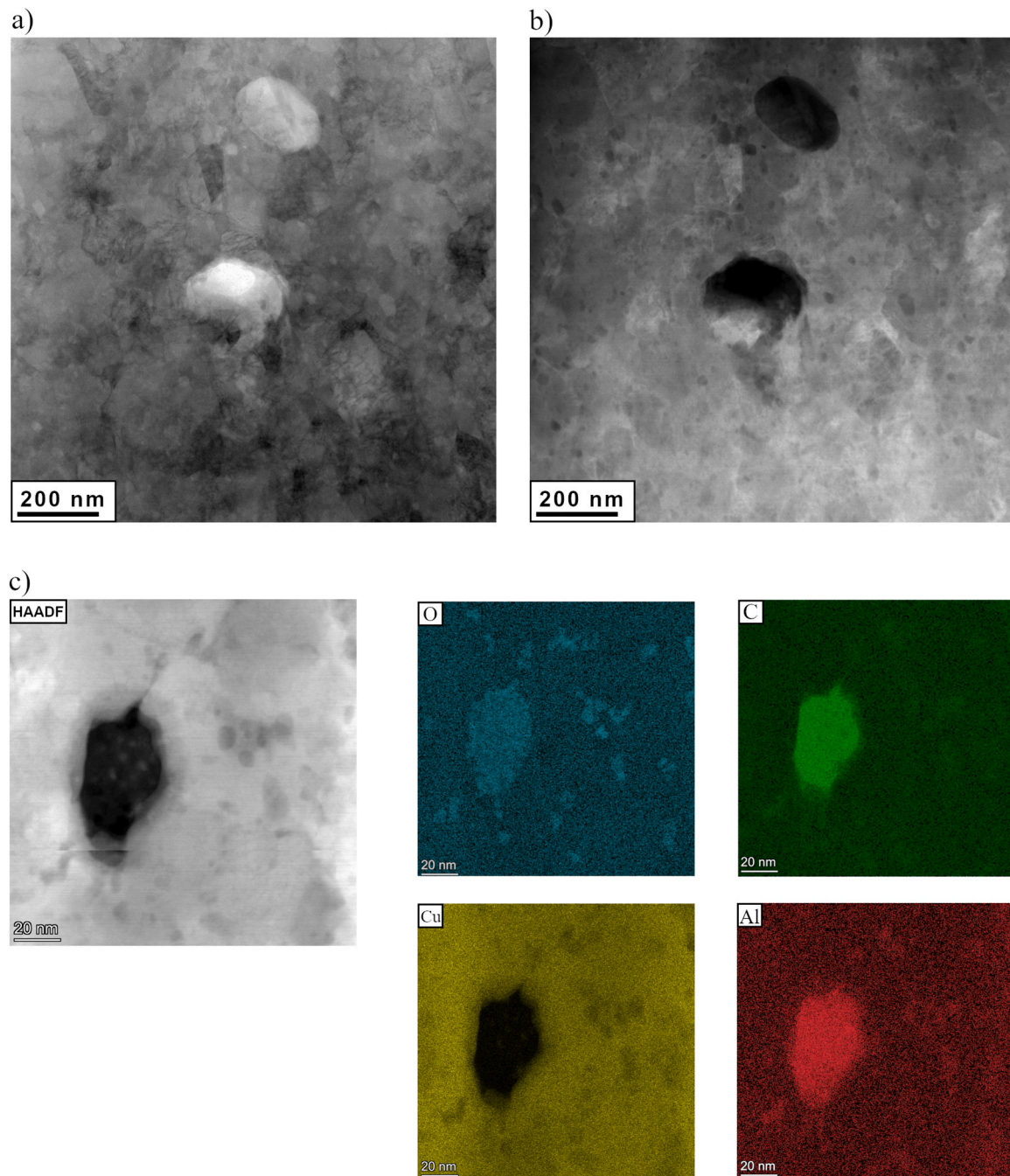


Fig. 4. STEM image of Cu-rGO/Al₂O₃ a) bright field, b) HAADF image, c) EDX map.

recrystallized grains are filled with small partial twins which are visible in the SEM image in Fig. 8d and were identified on the EBSD maps in Fig. 8(e-g). The EBSD maps presented in Fig. 8(e-g) reveal a very high density (85.4 %) of $\Sigma 3\{111\}$ twin boundaries, characterized by a misorientation angle of $60^\circ \pm 5^\circ$. Simultaneously, the grain orientation spread (GOS) and Kernel average misorientation (KAM) maps clearly indicate the absence of internal deformation within the observed grains. Both parameters exhibit very low values, confirming complete recrystallization. Furthermore, the presence of parallel, thin twin laths is typical of annealing twins. Considering the limitations of the EBSD technique, the dark lines observed in the band contrast maps are probably nanometric twins. However, due to the resolution limits of EBSD, these features cannot be directly detected.

In order to study the microstructural changes during annealing in

more detail, advanced investigations were carried out using STEM microscope. Fig. 9 presents representative STEM images of the Cu-GO, Cu-Al₂O₃ and Cu-rGO/Al₂O₃ microstructures after annealing at 773 K. In the Cu-GO composite (Fig. 9a) after annealing at 773 K there is minor grain growth, and the grain size increased from the HPT-processed value of ~ 55 nm to ~ 150 nm. In the microstructure of the Cu-GO composite, there is evidence for the formation of core-shell structures which are visible as dark regions on the HAADF images (Fig. 9a) and presented at higher magnification in Fig. 9b. The EDX analyses of these structures, summarized in Table 1, indicate that they consist of a carbon-rich core and an oxygen-rich shell zone embedded within the Cu matrix. The STEM images of the Cu-Al₂O₃ sample (Fig. 9c) demonstrate the excellent thermal stability of this composite with only a slight grain growth from the HPT-processed ~ 65 nm to ~ 110 nm after annealing at 773 K. The

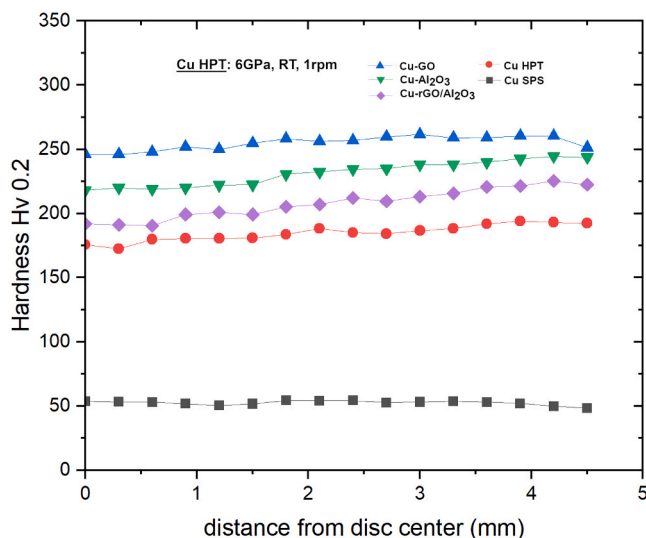


Fig. 5. Hardness measurements of the produced materials as a function of the distance from the disc centres.

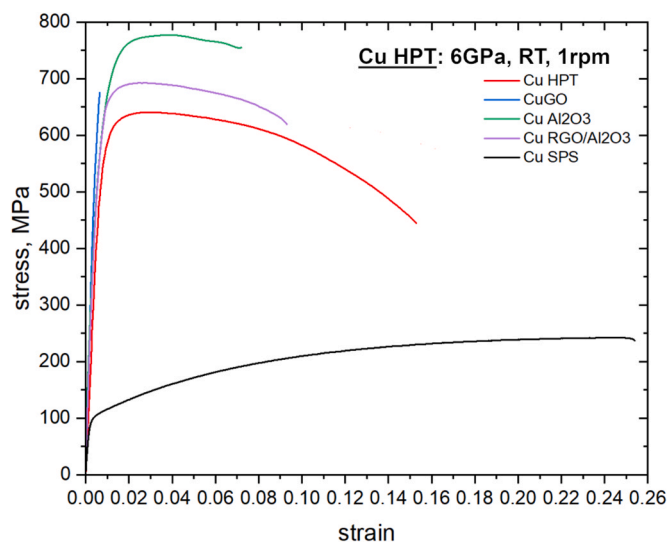


Fig. 6. Tensile strength results.

STEM images for the Cu-rGO/Al₂O₃ composite (Fig. 9d) reveal abnormal grain growth after annealing at 773 K and it is possible to distinguish a zone of finely refined grains with uniformly distributed nanoparticles together with the zone where recrystallization occurred. In these recrystallized regions numerous partial twins are observed, within which there are nanoparticles along the grain boundaries. In the nanocrystalline regions more rGO/Al₂O₃ particles are visible than in the recrystallized zones. Unlike the Cu-GO sample, where the core-shell structure of the C-rich core and the Cu-oxide layer were visible after annealing, in the Cu-rGO/Al₂O₃ composite this effect was not evident after the annealing.

4. Discussion

4.1. Effect of nanoparticle type on the microstructure and properties of composites

The addition of nanoparticles to a copper matrix has a great influence on the microstructure development during HPT processing and in the subsequent properties of the nanocomposites. The nanoparticles added

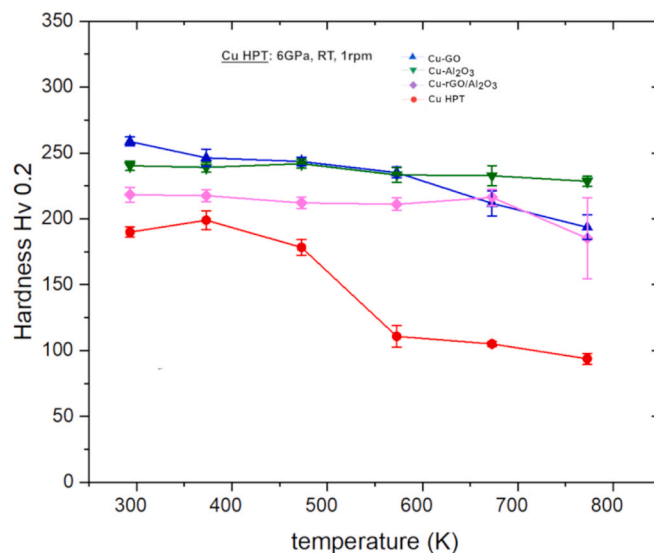


Fig. 7. Hardness as a function of annealing temperature.

in this study were GO, Al₂O₃ and rGO/Al₂O₃ and they all enhanced the grain refinement. The fabricated composites had nanocrystalline structures with average grain sizes ranging from ~55 to ~75 nm for Cu-GO, Cu-Al₂O₃ and Cu-rGO/Al₂O₃, respectively, while for pure Cu after HPT the grain size was ~210 nm. The substantial grain refinement observed in the composite materials during SPD processing is well-established and has been reported in various earlier studies [12,14,16]. The incorporation of stable, hard nanofillers and their uniform distribution within the metal matrix can restrict dislocation movement and pin grain boundaries, thereby effectively limiting their mobility. This suppresses dynamic recrystallization and recovery processes which occur during intense plastic deformation, shifting the structural saturation point [56] and ultimately enhancing the grain size refinement. It is worth noting that the saturation effect depends on the type of material, its purity, melting point or stacking fault energy. Furthermore, the saturation effect applies not only to the size of the grains, but also to the particles of the second phase. Research has shown that for a given material subjected to the HPT process, there is a certain level of saturation to which the material will aspire from both 'above' and 'below' [57–59].

Additionally, the uniform distribution of the reinforcing phase within the copper matrix has a crucial impact on both the microstructure and the mechanical properties. The Cu-GO and Cu-Al₂O₃ samples displayed the best reinforcement distribution, corresponding to the smallest grain sizes of the matrix. By contrast, the Cu-rGO/Al₂O₃ composite showed a higher degree of agglomeration, and this led to a less effective structural refinement.

These differences are primarily attributed to the distinct characteristics and structures of the reinforcing phases. Previous studies have shown that GO is less prone to agglomeration in a metal matrix compared to graphene or carbon nanotubes due to the presence of carboxyl and hydroxyl groups on the surface of GO [28–31]. These groups form Cu-O-C chemical bonds with the matrix, improving the dispersion of GO within the matrix and strengthening the bonding between the Cu matrix and the GO reinforcing phase. For composites reinforced with Al₂O₃ particles, the particles were initially nanosized with an average size of ~50 nm. As a result, the combination of milling and 20 HPT turns was sufficient to break most of the agglomerates and achieve an essentially uniform distribution of the Al₂O₃ particles in the Cu matrix. By contrast, for the rGO/Al₂O₃ particles, most of the carboxyl and hydroxyl groups originally present on the GO surface are used during the synthesis of the rGO/Al₂O₃ flakes as they form Al₂O₃-C bonds. This limits the ability of the rGO/Al₂O₃ flakes to bond effectively with the Cu matrix and, moreover, the rGO/Al₂O₃ flakes are stiffer and

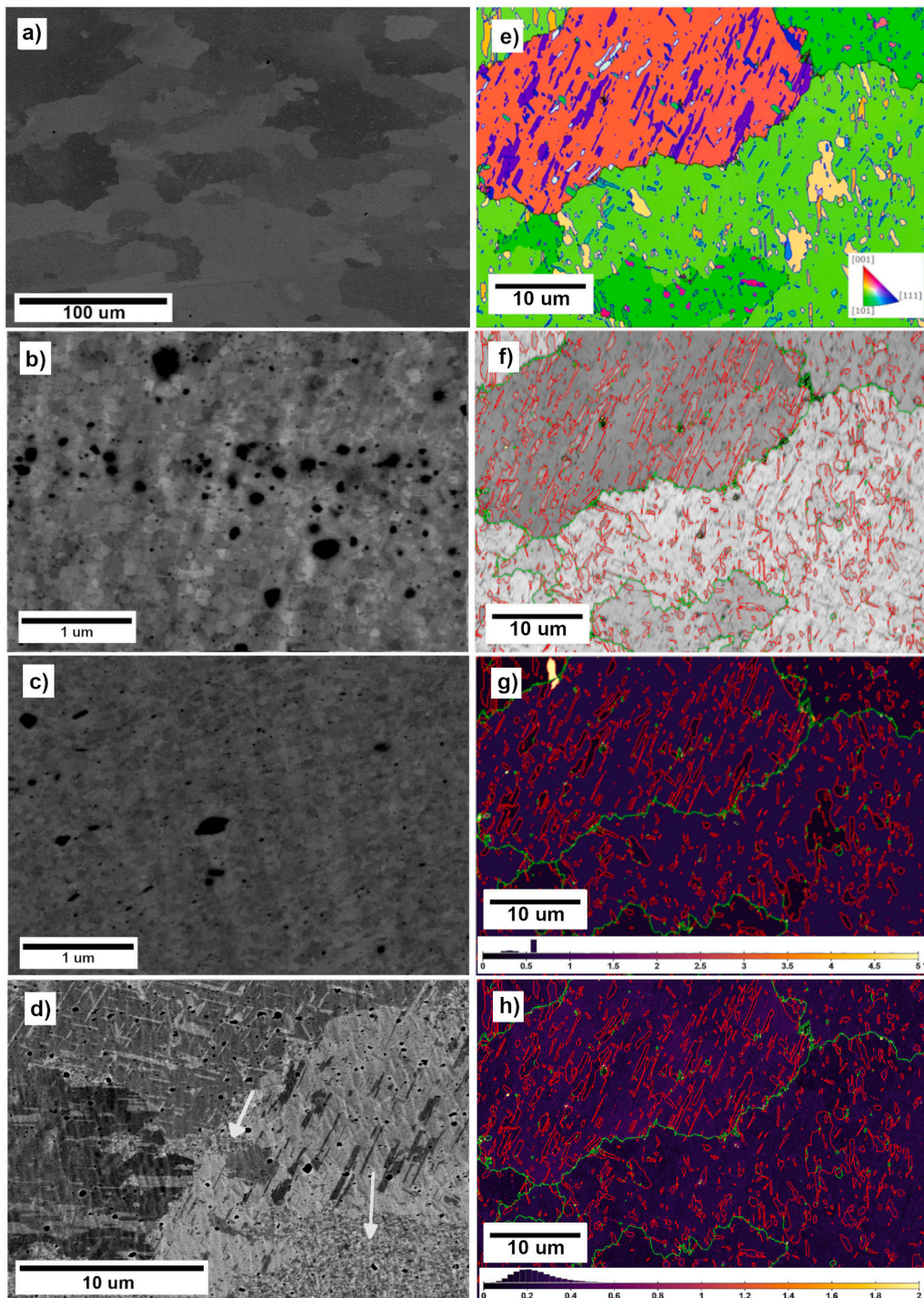


Fig. 8. SEM images of samples after annealing: a) Cu after HPT annealed at 573 K; b) Cu-GO annealed at 773 K; c) Cu-Al₂O₃ annealed at 773 K; d) Cu-rGO/Al₂O₃ annealed at 773 K; e) EBSD map of Cu-rGO/Al₂O₃ annealed at 773 K; f) EBSD band contrast map with marked $\Sigma 3$ twin boundaries (red), HAGB (green) and LAGB (yellow); g) EBSD grain orientation spread (GOS) map with marked $\Sigma 3$ twin boundaries (red), HAGB (green) and LAGB (yellow); h) EBSD Kernel average misorientation (KAM) map with marked $\Sigma 3$ twin boundaries (red), HAGB (green) and LAGB (yellow).

more difficult to break during processing so that their agglomerates are harder to fragment and uniformly distribute within the Cu matrix [60].

The composites fabricated in this research exhibit unique hardness (Fig. 5) when compared with the coarse-grained and nanostructured pure copper. The hardness values increased by appropriately 200 % for the Cu-rGO/Al₂O₃ composite, 230 % for Cu-Al₂O₃ and 250 % for the Cu-GO composite relative to the initial coarse-grained copper. This unique enhancement in mechanical properties is attributed to several factors: a) the significant grain size reduction which is consistent with the Hall-

Petch relationship [57,61], b) the presence of hard, uniformly distributed GO, Al₂O₃ and rGO/Al₂O₃ nanoparticles within the matrix [58] and c) the increased dislocation density caused by additional obstacles to dislocation movement. The observed differences in microhardness values between the samples are a consequence of the varying degrees of grain size reduction, the distribution of the reinforcement phase within the matrix and the level of nanoparticle agglomeration.

The UTS of the fabricated nanocomposites (Fig. 6) ranged from 675 MPa to 780 MPa and these values are nearly three times higher than

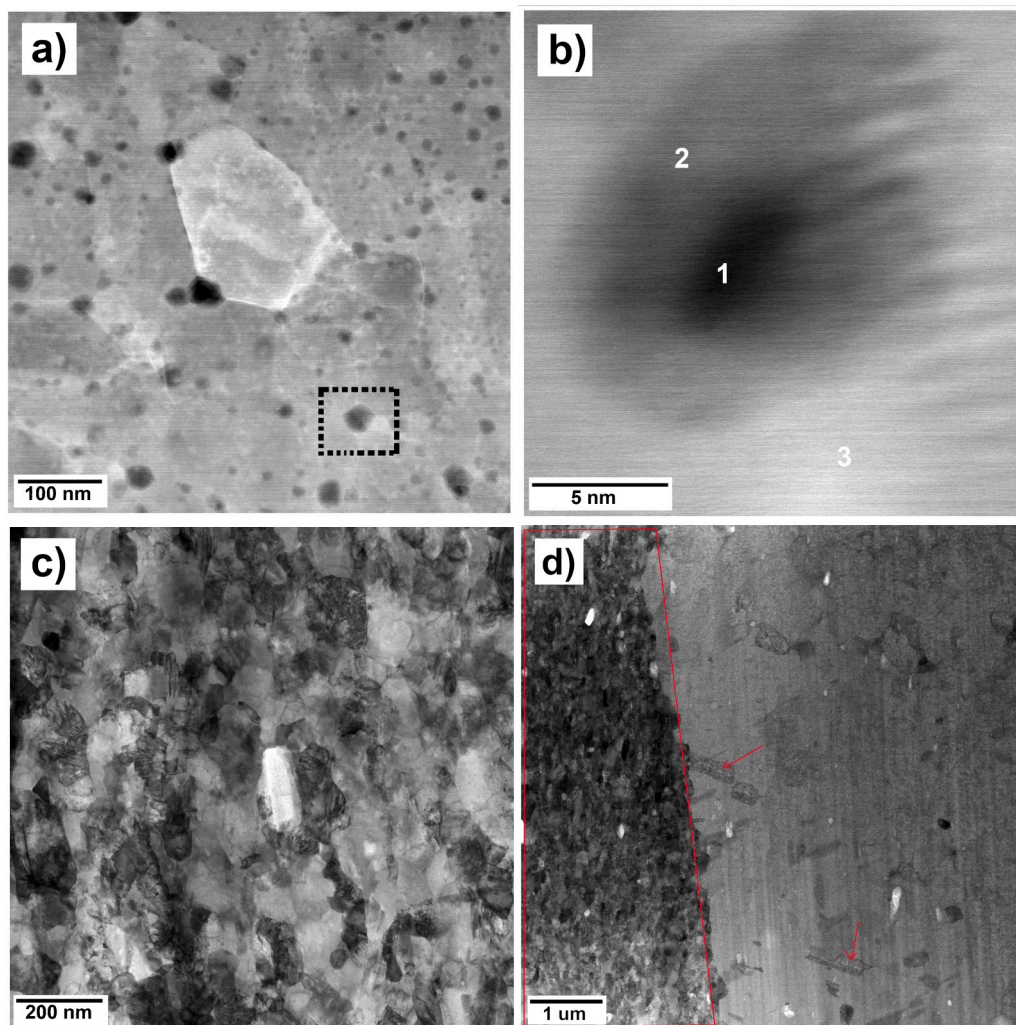


Fig. 9. SEM images of samples after annealing at 773 K: a) Cu-GO; b) higher magnification of the area marked by the square in a), numbers indicate Cu-GO EDS measure points (1 - C; 2 - O; 3 - Cu); c) Cu-Al₂O₃; d) Cu-rGO/Al₂O₃.

Table 1
EDX measurements correlated with STEM image - Fig. 9b.

	C-K	O-K	Cu-K
Point 1	14.3	43.4	45.3
Point 2	2.5	33.2	64.3
Point 3	0.9	3.4	95.7

for unprocessed copper (~250 MPa) and 40 MPa to 140 MPa higher than HPT-processed Cu. The highest UTS was observed in the Cu-Al₂O₃ sample (~780 MPa) and the Cu-rGO/Al₂O₃ sample (~690 MPa). Both samples also demonstrated plasticity in the range of 6–8%. This enhanced strength is attributed to significant grain refinement and the presence of hard particles that hinder dislocation movement. The sample with the GO addition, despite exhibiting the highest hardness, could not be evaluated in tensile testing due to their failure in the elastic region. This problem has been widely discussed and is generally attributed to two factors. First, the Cu-GO microstructure experiences intense grain size reduction, with the smallest grain size of 55 nm reported for this sample, and this leads to a lack of accommodation of stress through plastic deformation and therefore to premature failure during testing [59]. Second, the exceptionally small sizes of the tensile test samples (4.0 × 0.6 × 0.8 mm³) which were cut using an EDM machine. The surface roughness of such tensile samples is enhanced and this, combined

with their small dimensions, may have led to the formation of localized stress concentrations causing early failure under tension.

4.2. Thermal stability of the composites

The addition of nanoparticles to the copper matrix significantly influences not only grain refinement and the mechanical properties but also the thermal stability of the composites. The particles restrict the movement of grain boundaries during annealing and actively inhibit recrystallization in the Zener pinning effect [62]. In this context, the thermal behaviour of the fillers and their uniform distribution within the copper matrix are critical factors determining the thermal stability of these nanocomposites.

As shown in Fig. 7, the produced composites are thermally stable up to at least 673 K where this is significantly greater than for pure copper after HPT (473 K). At elevated temperatures, notable differences begin to emerge between the composites. Starting from the Cu-Al₂O₃ composite, it remains thermally stable up to 773 K with both the microstructure and the microhardness remaining stable throughout the entire temperature range. This is attributed to the presence of a uniformly distributed Al₂O₃ in the matrix (Fig. 3) and thermally stable Al₂O₃ nanoparticles with a diameter of 6.5 nm which act as effective barriers for grain growth. This mechanism is well documented in the literature [20,26,63,23].

The addition of GO gave the highest hardness and the smallest grain

size among all fabricated composites. However, the Cu-GO composite exhibited a slight drop of hardness as the temperature increased. After annealing at 773 K the hardness dropped from 260 Hv units to approximately 190 Hv units. It is worth noting that this value is comparable to that of pure copper after HPT processing. The drop of mechanical properties is associated with specific microstructural changes occurring in the sample after annealing at 773 K (Fig. 8 and Fig. 9). Firstly, limited grain growth was observed, with the grain size increasing from the HPT-processed ~55 nm to ~150 nm. Secondly, the GO nanoparticles transformed into core-shell structures embedded within the metal matrix, consisting of an oxygen-rich outer layer and a carbon-rich core (Fig. 9). These core-shell structures are less effective in inhibiting grain growth compared to the Al₂O₃ nanoparticles and their formation is linked to the degradation of GO at higher temperatures. During heating, oxygen functional groups on the GO surface react with the Cu matrix to form diffusive layers of CuO and CuO₂. Subsequently, the hexagonal graphene structure degrades, leading to the formation of a graphite core [54,64-66].

The composite with the addition of rGO/Al₂O₃ seems to be thermally stable up to 673 K and the annealing at 773 K produced abnormal grain growth and the formation of a heterostructure composed of large recrystallized grains (Fig. 8d) containing partial recrystallization twins (marked with red arrows Fig. 9d) which were identified based on the EBSD analysis (Fig. 8e) and some nanocrystalline regions (indicated by white arrows on Fig. 8d and red frame Fig. 9d). This heterostructure formation is attributed to an inhomogeneous distribution of rGO/Al₂O₃ particles in the matrix. The fabrication of rGO/Al₂O₃ nanoparticles significantly increased the stiffness and strength of the GO flakes preventing many of them from fragmenting during the HPT processing (Fig. 1d and Fig. 4). Therefore, large agglomerates remained in the microstructure, and this reduced the number of obstacles to recrystallization leading to a partial recrystallization. Moreover, there was no trace of the formation of a core-shell structure typical of the GO sample. This is associated with the production route of rGO/Al₂O₃ which already included a thermal treatment at 553 K for 2 h which effectively decomposed the organic precursor to Al₂O₃ and reduced the GO to rGO [50]. The GO poses oxygen-containing functional groups on its surface such as carbonyl, epoxy, carboxylic acid and hydroxyl which decompose during annealing [64] and cause the formation of a core-shell structure in the Cu-GO sample. When these oxygen groups are reduced, the material becomes rGO and this material is thermally stable even above 1273 K [64]. For the rGO/Al₂O₃ nanoparticles, there are no free oxygen-containing functional groups which are capable of decomposing during annealing of the Cu-rGO/Al₂O₃ samples.

5. Conclusions

The type of nanofiller and its distribution in the copper matrix has a significant effect on the microstructure, mechanical properties and thermal stability of the composite. Analysis of the microstructure in terms of grain size showed that the greatest difference is attributed to the presence of nanofillers as the copper without additives had grain sizes of the order of ~210 nm whereas the composites had grain sizes of ~55 nm, ~65 nm and ~75 nm for Cu-GO, Cu-Al₂O₃ and Cu-rGO/Al₂O₃, respectively.

The type of additive influenced the extent by which the hardness improved by comparison with copper after HPT. These improvements increased by 65 Hv, 45 Hv and 25 Hv for Cu-GO, Cu-Al₂O₃ and Cu-rGO/Al₂O₃, respectively. Significant differences were also seen in the tensile tests where the Cu-GO composite cracked in the elastic range while the other composites showed some plastic deformation range with higher UTS values of ~780 MPa in Cu-Al₂O₃ and ~690 MPa in Cu-rGO/Al₂O₃ compared with ~640 MPa in Cu after HPT.

The greatest difference between the additives was observed in the thermal stability tests. The Cu-Al₂O₃ composite annealed at 373 – 773 K had almost the same hardness and its microstructure changed slightly

such that, after annealing at 773 K, the average grain size increased to ~100 nm. The Cu-GO composite showed a slow and minor decrease in hardness with increasing annealing temperature and the hardness decreased to ~180 Hv after annealing at 773 K. There were more observable changes in the microstructure of this composite related to the thermal decomposition of GO but the grain size increased to only ~150 nm and therefore the material remained in the UFG condition. The Cu-rGO/Al₂O₃ composite remained stable in terms of hardness and microstructure up to 673 K but annealing at 773 K led to a decrease in hardness to ~185 Hv associated with microstructural growth. It is noteworthy that the composite underwent abnormal grain growth resulting in a bimodal structure caused by an uneven distribution of reinforcing particles in the matrix.

It is also worth emphasising that all the produced composites had better thermal stability than the HPT-processed pure Cu and their hardness values after annealing at 773 K were higher than for Cu after HPT without subsequent annealing.

CRedit authorship contribution statement

Bednarczyk Witor: Investigation. **Marta Ciemiorek:** Investigation. **Anita Wojciechowska:** Investigation. **Yi Huang:** Writing – review & editing, Validation, Investigation. **Terence G. Langdon:** Writing – review & editing, Supervision, Conceptualization. **Małgorzata Lewandowska:** Writing – review & editing, Conceptualization. **Agnieszka Jastrzębska:** Writing – review & editing. **Maria Emerla:** Writing – original draft, Methodology, Investigation, Data curation. **Piotr Bazarnik:** Writing – original draft, Project administration, Methodology, Investigation, Funding acquisition, Data curation, Conceptualization.

Declaration of Competing Interest

The authors declare that they have no known competing financial interests or personal relationships that could have appeared to influence the work reported in this paper.

Acknowledgments

This work was carried out within an OPUS 19 project “Metal matrix composites fabricated by high-pressure torsion and reinforced with 2D and 3D nano-particles” funded by National Science Centre under nb. 2020/37/B/ST5/01837.

Data availability

Most of the data on which this article is based has been included. Other measurement data and numerous microscopic images produced during the research can be made available on request to the reader by contacting the corresponding author.

References

- [1] Q. Mao, Y. Liu, Y. Zhao, A review on copper alloys with high strength and high electrical conductivity, *J. Alloy. Compd.* 990 (2024) 174456, <https://doi.org/10.1016/j.jallcom.2024.174456>.
- [2] M. Lipińska, P. Bazarnik, M. Lewandowska, The influence of severe plastic deformation processes on electrical conductivity of commercially pure aluminium and 5483 aluminium alloy, *Arch. Civ. Mech. Eng.* 16 (2016) 717–723, <https://doi.org/10.1016/j.acme.2016.04.013>.
- [3] Y. Iwahashi, Z. Horita, M. Nemoto, T.G. Langdon, The process of grain refinement in equal-channel angular pressing, *Acta Met.* 46 (1998) 3317–3331, [https://doi.org/10.1016/S1359-6454\(97\)00494-1](https://doi.org/10.1016/S1359-6454(97)00494-1).
- [4] H.N. Omran, A.R. Eivani, M. Farbakhti, H.R. Jafarian, Tribological properties of copper-graphene (CuG) composite fabricated by accumulative roll bonding, *J. Mater. Res. Technol.* 25 (2023) 4650–4657, <https://doi.org/10.1016/j.jmrt.2023.06.261>.
- [5] A. Vorhauer, R. Pippan, On the homogeneity of deformation by high pressure torsion, *Scr. Mater.* 51 (2004) 921–925, <https://doi.org/10.1016/j.scriptamat.2004.04.025>.

- [6] S. Sabbaghianrad, J. Wongsang-ngam, M. Kawasaki, T.G. Langdon, An examination of the saturation microstructures achieved in ultrafine-grained metals processed by high-pressure torsion, *J. Mater. Res. Technol.* 3 (2014) 319–326, <https://doi.org/10.1016/j.jmrt.2014.10.002>.
- [7] Y. Ito, K. Edalati, Z. Horita, High-pressure torsion of aluminum with ultrahigh purity (99.9999%) and occurrence of inverse Hall-Petch relationship, *Mater. Sci. Eng. A* 679 (2017) 428–434, <https://doi.org/10.1016/j.msea.2016.10.066>.
- [8] A.P. Zhilyaev, T.G. Langdon, Using high-pressure torsion for metal processing: Fundamentals and applications, *Prog. Mater. Sci.* 53 (2008) 893–979, <https://doi.org/10.1016/j.pmatsci.2008.03.002>.
- [9] M. Kawasaki, H.J. Lee, B. Ahn, A.P. Zhilyaev, T.G. Langdon, Evolution of hardness in ultrafine-grained metals processed by high-pressure torsion, *J. Mater. Res. Technol.* 3 (2014) 311–318, <https://doi.org/10.1016/j.jmrt.2014.06.002>.
- [10] K. Edalati, K. Imamura, T. Kiss, Z. Horita, Equal-channel angular pressing and high-pressure torsion of pure copper: evolution of electrical conductivity and hardness with strain, *Mater. Trans.* 53 (2012) 123–127, <https://doi.org/10.2320/matertrans.MD201109>.
- [11] H. Jiang, Y.T. Zhu, D.P. Butt, I.V. Alexandrov, T.C. Lowe, Microstructural evolution, microhardness and thermal stability of HPT-processed Cu, *Mater. Sci. Eng. A* 290 (2000) 128–138, [https://doi.org/10.1016/S0921-5093\(00\)00919-9](https://doi.org/10.1016/S0921-5093(00)00919-9).
- [12] R.Z. Valiev, R.K. Islamgaliev, I.V. Alexandrov, 2000, Bulk nanostructured materials from severe plastic deformation, 2000. [https://doi.org/10.1016/S0079-6425\(99\)00007-9](https://doi.org/10.1016/S0079-6425(99)00007-9).
- [13] R.K. Islamgaliev, F. Chmelik, R. Kuzel, Thermal structure changes in copper and nickel processed by severe plastic deformation, 335–338, *Mater. Sci. Eng. A* (1997) 234–236, [https://doi.org/10.1016/S0921-5093\(97\)00247-5](https://doi.org/10.1016/S0921-5093(97)00247-5).
- [14] J. Čížek, I. Procházková, M. Cieslar, R. Kuzel, J. Kuriplach, F. Chmelík, I. Stulíková, F. Bečvář, O. Melikhova, R.K. Islamgaliev, Thermal stability of ultrafine grained copper, *Phys. Rev. B - Condens. Matter Mater. Phys.* 65 (2002) 1–16, <https://doi.org/10.1103/PhysRevB.65.094106>.
- [15] N. Lugo, N. Llorca, J.J. Sunol, J.M. Cabrera, Thermal stability of ultrafine grains size of pure copper obtained by equal-channel angular pressing, *J. Mater. Sci.* 45 (2010) 2264–2273, <https://doi.org/10.1007/s10853-009-4139-7>.
- [16] J. Čížek, I. Procházková, M. Cieslar, R.K. Islamgaliev, O. Kulyasova, Influence of ceramic nanoparticles on thermal stability of ultra fine grained copper, *Acta Phys. Pol. A* 113 (2008) 1285–1292, <https://doi.org/10.12693/APhysPolA.113.1285>.
- [17] B. Tian, P. Liu, K. Song, Y. Li, Y. Liu, F. Ren, J. Su, Microstructure and properties at elevated temperature of a nano-Al₂O₃ particles dispersion-strengthened copper base composite, 705–710, *Mater. Sci. Eng. A* (2006) 435–436, <https://doi.org/10.1016/j.msea.2006.07.129>.
- [18] D. Shen, P. Gao, Y. He, J. Gong, J. Du, A Cu-Al₂O₃ composite with ultrahigh tensile strength prepared by high-pressure torsion, *J. Mater. Eng. Perform.* (2022) 1–6, <https://doi.org/10.1007/s11665-022-06936-9>.
- [19] J. Naser, H. Ferkel, W. Riehemann, Grain stabilisation of copper with nanoscaled Al₂O₃-powder, 470–473, *Mater. Sci. Eng. A* (1997) 234–236, [https://doi.org/10.1016/S0921-5093\(97\)00263-3](https://doi.org/10.1016/S0921-5093(97)00263-3).
- [20] H.R. Peng, M.M. Gong, Y.Z. Chen, F. Liu, Thermal stability of nanocrystalline materials: thermodynamics and kinetics, *Int. Mater. Rev.* 62 (2017) 303–333, <https://doi.org/10.1080/09506608.2016.1257536>.
- [21] P.A. Manohar, M. Ferry, T. Chandra, Five decades of the Zener Equation, *ISIJ Int* 38 (1998) 913–924, <https://doi.org/10.2355/isijinternational.38.913>.
- [22] N. Wang, Y. Wen, L.Q. Chen, Pinning force from multiple second-phase particles in grain growth, *Comput. Mater. Sci.* 93 (2014) 81–85, <https://doi.org/10.1016/j.commatsci.2014.06.030>.
- [23] E. Nes, N. Ryum, O. Hunderi, On the Zener Drag, *Acta Metallurgica* 33 (1985) 11–22.
- [24] D. Li, S. Zhou, P. Li, W. Lü, X. Zhu, Research progresses on thermal stabilization of metal nanocrystalline alloys, *Xiyou Jinshu Cailiao Yu Gongcheng/Rare Met. Mater. Eng.* 44 (2015) 1075–1081, [https://doi.org/10.1016/S1875-5372\(15\)30070-9](https://doi.org/10.1016/S1875-5372(15)30070-9).
- [25] R.Z. Valiev, R.K. Islamgaliev, N.F. Kuzmina, Y. Li, T.G. Langdon, Strengthening and grain refinement in an Al-6061 metal matrix composite through intense plastic straining, *Scr. Mater.* 40 (1999) 117–122, [https://doi.org/10.1016/S1359-6462\(98\)00398-4](https://doi.org/10.1016/S1359-6462(98)00398-4).
- [26] D. Zhou, D. Zhang, C. Kong, P. Munroe, R. Torrens, Grain and nanoparticle coarsening of an ultrafine structured Cu-5 vol%Al₂O₃ nanocomposite during isochronal annealing, *J. Alloy. Compd.* 642 (2015) 83–91, <https://doi.org/10.1016/j.jallcom.2015.04.106>.
- [27] K. Edalati, M. Ashida, Z. Horita, T. Matsui, H. Kato, Wear resistance and tribological features of pure aluminum and Al-Al₂O₃ composites consolidated by high-pressure torsion, *Wear* 310 (2014) 83–89, <https://doi.org/10.1016/j.wear.2013.12.022>.
- [28] M.I. Abd El Aal, Wear properties of copper and copper composites powders consolidated by high-pressure torsion, *Friction* 8 (2020) 433–450, <https://doi.org/10.1007/s40544-019-0285-3>.
- [29] M. Jahedi, M.H. Paydar, M. Knezevic, Enhanced microstructural homogeneity in metal-matrix composites developed under high-pressure-double-torsion, *Mater. Charact.* 104 (2015) 92–100, <https://doi.org/10.1016/j.matchar.2015.04.012>.
- [30] M.I. Abd El Aal, Effect of high-pressure torsion processing on the microstructure evolution and mechanical properties of consolidated micro size Cu and Cu-SiC powders, *Adv. Powder Technol.* 28 (2017) 2135–2150, <https://doi.org/10.1016/j.apt.2017.05.020>.
- [31] P. Hidalgo-Manrique, X. Lei, R. Xu, M. Zhou, I.A. Kinloch, R.J. Young, Copper/graphene composites: a review, *J. Mater. Sci.* 54 (2019) 12236–12289, <https://doi.org/10.1007/s10853-019-03703-5>.
- [32] P. Jenei, E.Y. Yoon, J. Gubicza, H.S. Kim, J.L. Lábár, T. Ungár, Microstructure and hardness of copper-carbon nanotube composites consolidated by High Pressure Torsion, *Mater. Sci. Eng. A* 528 (2011) 4690–4695, <https://doi.org/10.1016/j.msea.2011.02.066>.
- [33] S.K. Tiwari, H. Singh, A. Midathada, S. Sharma, U.K. Ravella, Study of Fabrication Processes and Properties of Al-CNT Composites Reinforced by Carbon Nano tubes—A Review, *Mater. Today Proc.* 5 (2018) 28262–28270, <https://doi.org/10.1016/j.matpr.2018.10.109>.
- [34] T. Tokunaga, K. Kaneko, Z. Horita, Production of aluminum-matrix carbon nanotube composite using high pressure torsion, *Mater. Sci. Eng. A* 490 (2008) 300–304, <https://doi.org/10.1016/j.msea.2008.02.022>.
- [35] C. Xiong, D. Li, S. Song, Y. Ye, Z. Ye, D. Zuo, Research on the performance of rGO-CNTs synergistically enhanced copper matrix composites, *Powder Technol.* 394 (2021) 1–9, <https://doi.org/10.1016/j.powtec.2021.08.007>.
- [36] N. Khobragade, K. Sikdar, B. Kumar, S. Bera, D. Roy, Mechanical and electrical properties of copper-graphene nanocomposite fabricated by high pressure torsion, *J. Alloy. Compd.* 776 (2019) 123–132, <https://doi.org/10.1016/j.jallcom.2018.10.139>.
- [37] J. Hwang, T. Yoon, S.H. Jin, J. Lee, T.S. Kim, S.H. Hong, S. Jeon, Enhanced mechanical properties of graphene/copper nanocomposites using a molecular-level mixing process, *Adv. Mater.* 25 (2013) 6724–6729, <https://doi.org/10.1002/adma.201302495>.
- [38] K. Zhang, Fabrication of copper nanoparticles/graphene oxide composites for surface-enhanced Raman scattering, *Appl. Surf. Sci.* 258 (2012) 7327–7329, <https://doi.org/10.1016/j.apsusc.2012.04.002>.
- [39] F. Lin, R. Xu, M. Zhou, R.J. Young, I.A. Kinloch, Y. Ding, Mechanical and Electrical Properties of Graphene Oxide Reinforced Copper-Tungsten Composites Produced via Ball Milling of Metal Flakes, *Mater. (Basel)* 15 (2022), <https://doi.org/10.3390/ma15217736>.
- [40] P. Jenei, J. Gubicza, E.Y. Yoon, H.S. Kim, J.L. Lábár, High temperature thermal stability of pure copper and copper-carbon nanotube composites consolidated by High Pressure Torsion, *Compos. Part A Appl. Sci. Manuf.* 51 (2013) 71–79, <https://doi.org/10.1016/j.compositesa.2013.04.007>.
- [41] G. Giovannetti, P.A. Khomyakov, G. Brocks, V.M. Karpan, J. Van Den Brink, P. J. Kelly, Doping graphene with metal contacts, *Phys. Rev. Lett.* 101 (2008) 4–7, <https://doi.org/10.1103/PhysRevLett.101.026803>.
- [42] P.A. Khomyakov, G. Giovannetti, P.C. Rusu, G. Brocks, J. Van Den Brink, P.J. Kelly, First-principles study of the interaction and charge transfer between graphene and metals, *Phys. Rev. B - Condens. Matter Mater. Phys.* 79 (2009) 1–12, <https://doi.org/10.1103/PhysRevB.79.195425>.
- [43] L. Zhang, E. Pollak, W.C. Wang, P. Jiang, P.A. Glans, Y. Zhang, J. Cabana, R. Kostecki, C. Chang, M. Salmeron, J. Zhu, J. Guo, Electronic structure study of ordering and interfacial interaction in graphene/Cu composites, *Carbon N. Y* 50 (2012) 5316–5322, <https://doi.org/10.1016/j.carbon.2012.07.020>.
- [44] K. Raidongia, A.T.L. Tan, J. Huang, Graphene Oxide: Some New Insights into an Old Material, Second Edi, Elsevier Ltd, 2014, <https://doi.org/10.1016/B978-0-08-098232-8.00014-0>.
- [45] I. Sengupta, S. Chakraborty, M. Talukdar, S.K. Pal, S. Chakraborty, Thermal reduction of graphene oxide: How temperature influences purity, *J. Mater. Res.* 33 (2018) 4113–4122, <https://doi.org/10.1557/jmr.2018.338>.
- [46] I. Sengupta, S.S.S. Sharat Kumar, S.K. Pal, S. Chakraborty, Characterization of structural transformation of graphene oxide to reduced graphene oxide during thermal annealing, *J. Mater. Res.* 35 (2020) 1197–1204, <https://doi.org/10.1557/jmr.2020.55>.
- [47] B.S. Kong, J. Geng, H.T. Jung, Layer-by-layer assembly of graphene and gold nanoparticles by vacuum filtration and spontaneous reduction of gold ions, *Chem. Commun.* (2009) 2174–2176, <https://doi.org/10.1039/b821920f>.
- [48] X. Zhou, X. Huang, X. Qi, S. Wu, C. Xue, F.Y.C. Boey, Q. Yan, P. Chen, H. Zhang, In situ synthesis of metal nanoparticles on single-layer graphene oxide and reduced graphene oxide surfaces, *J. Phys. Chem. C* 113 (2009) 10842–10846, <https://doi.org/10.1021/jp903821n>.
- [49] Y. Liang, H. Wang, H.S. Casalongue, Z. Chen, H. Dai, TiO₂ nanocrystals grown on graphene as advanced photocatalytic hybrid materials, *Nano Res.* 3 (2010) 701–705, <https://doi.org/10.1007/s12274-010-0033-5>.
- [50] A.M. Jastrzębska, J. Karcz, R. Letmanowski, D. Zabost, E. Ciecierska, J. Zdunek, E. Karwowska, M. Siekierski, A. Olszyna, A. Kunicki, Synthesis of the RGO/Al₂O₃ core-shell nanocomposite flakes and characterization of their unique electrostatic properties using zeta potential measurements, *Appl. Surf. Sci.* 362 (2016) 577–594, <https://doi.org/10.1016/j.apsusc.2015.10.125>.
- [51] N. Kurantowicz, E. Sawosz, S. Jaworski, M. Kutwin, B. Strojny, M. Wierzbicki, J. Szeliga, A. Hotowy, L. Lipińska, R. Koziołski, J. Jagielto, A. Chwalibog, Interaction of graphene family materials with *Listeria monocytogenes* and *Salmonella enterica*, *Nanoscale Res. Lett.* 10 (2015) 1–12, <https://doi.org/10.1186/s11671-015-0749-y>.
- [52] A.M. Jastrzębska, E. Karwowska, A. Tabernacka, P. Mosdorf, P. Polis, P. Kurtycz, A. Olszyna, A.R. Kunicki, New non phyto- and eco-toxic alumina-stabilized silver and praseodymium nanoparticles, *Int. J. Appl. Ceram. Technol.* 10 (2013) 908–916, <https://doi.org/10.1111/j.1744-7402.2012.02834.x>.
- [53] R.B. Figueiredo, P.H.R. Pereira, M.T.P. Aguiar, P.R. Cetlin, T.G. Langdon, Using finite element modeling to examine the temperature distribution in quasi-constrained high-pressure torsion, *Acta Mater.* 60 (2012) 3190–3198, <https://doi.org/10.1016/j.actamat.2012.02.027>.
- [54] V.V. Popova, A.V. Stolbovkiy, E.N. Popova, V.P. Pilyugin, Structure and thermal stability of Cu after severe plastic deformation, 1312–1321, *Defect Diffus. Forum* (2010) 297–301, <https://doi.org/10.4028/www.scientific.net/DDF.297-301.1312>.
- [55] M. Emerla, P. Bazarnik, Y. Huang, A. Wojciechowska, M. Ciemiorek, J. Pura, M. Wiczorek-Czarnocka, P.M.A. Kenichi, A. Jastrzębska, M. Lewandowska, T. G. Langdon, The influence of graphene oxide on the microstructure and properties

- of ultrafine-grained copper processed by high-pressure torsion, *J. Alloy. Compd.* 1005 (2024), <https://doi.org/10.1016/j.jallcom.2024.176208>.
- [56] P. Bazarnik, S. Nosewicz, B. Romelczyk-Baishya, M. Chmielewski, A. Strojny Nędza, J. Maj, Y. Huang, M. Lewandowska, T.G. Langdon, Effect of spark plasma sintering and high-pressure torsion on the microstructural and mechanical properties of a Cu–SiC composite, *Mater. Sci. Eng. A* 766 (2019), <https://doi.org/10.1016/j.msea.2019.138350>.
- [57] H. Wen, R.K. Islamgaliev, K.M. Nesterov, R.Z. Valiev, E.J. Lavernia, Dynamic balance between grain refinement and grain growth during high-pressure torsion of Cu powders, *Philos. Mag. Lett.* 93 (2013) 481–489, <https://doi.org/10.1080/09500839.2013.805268>.
- [58] B.B. Straumal, R. Kulagin, L. Klinger, E. Rabkin, P.B. Straumal, O.A. Kogtenkova, B. Baretzky, Structure refinement and fragmentation of precipitates under severe plastic deformation: a review, *Mater. (Basel)* 15 (2022), <https://doi.org/10.3390/ma15020601>.
- [59] L. Upadhayay, S. Nilawar, C. Kumar, K. Chatterjee, P. Kumar, Effect of processing Mg–6Zn–0.2Ce through high-pressure torsion on its use as a biomaterial, *J. Mater. Sci.* 59 (2024) 5872–5890, <https://doi.org/10.1007/s10853-024-09460-4>.
- [60] Y. Hu, Y. Xie, H. Xin, J. Chen, shizhong, Y. Liu, C. Li, Xu, Nano/microstructures and mechanical properties of Al₂O₃–TiC ceramic composites reinforced with Al₂O₃@RGO nanohybrids, *Ceram. Int.* 48 (2022) 27536–27549, <https://doi.org/10.1016/j.ceramint.2022.06.047>.
- [61] M. Emerla, P. Bazarnik, Y. Huang, M. Lewandowska, T.G. Langdon, Using direct high-pressure torsion synthesis to produce aluminium matrix nanocomposites reinforced with carbon nanotubes, *J. Alloy. Compd.* 968 (2023), <https://doi.org/10.1016/j.jallcom.2023.171928>.
- [62] E.O. Hall, The deformation and ageing of mild steel III discussion of results, *Proc. Phys. Soc. Sect. B.* 64 (1951) 747–753.
- [63] N.J. Petch, The cleavage strength of polycrystals, *J. Iron Steel Inst.* 174 (1953) 25–28.
- [64] Y. Nishida, Introduction to Metal Matrix Composites, Springer Japan, Japan, 2013, <https://doi.org/10.1007/978-4-431-54237-7>.
- [65] Y. Estrin, A. Vinogradov, Extreme grain refinement by severe plastic deformation: A wealth of challenging science, *Acta Mater.* 61 (2013) 782–817, <https://doi.org/10.1016/j.actamat.2012.10.038>.
- [66] L. Hu, A. Wang, W. Wang, Structural Evolution of Graphene Oxide and Its Thermal Stability During High Temperature Sintering, *J. Wuhan. Univ. Technol. Mater. Sci. Ed.* 37 (2022) 342–349, <https://doi.org/10.1007/s11595-022-2537-8>.